Large Diameter Pulsating Heat Pipe for Future Experiments on the International Space Station: Ground and Microgravity Thermal Response

Mauro Mameli[1], Andrea Catarsi[1], Daniele Mangini[2], Luca Pietrasanta[2], Davide Fioriti[1], Marco La Foresta[3], Lorenzo Caporale[3], Nicolas Miche[2], Marco Marengo[2], Paolo Di Marco[1], Sauro Filippeschi[1]

[1]*University of Pisa, Largo Lucio Lazzarino 2, 56122 Pisa, Italy.*
[2] *School of Computing, Engineering and Mathematics, University of Brighton, Lewes Rd, Brighton BN2 4AT, UK.*
[3]*AAVID Thermalloy, Via del Fonditore, 4, 40138, Bologna, Italy.*

Abstract

This work describes the thermal characterization on ground and under a varying gravity field (parabolic flights) of a large diameter Pulsating Heat Pipe (PHP) especially designed for its future implementation on the heat transfer host module of the International Space Station (ISS) for long term microgravity experiments. A multi-turn compact closed loop PHP is made of aluminum and partially filled with FC-72 (50% vol.). The 3mm tube internal diameter is larger than the static capillary limit evaluated on ground conditions for the above working fluid, with the objective of dissipating larger heat power inputs compared to smaller diameter channels, under microgravity conditions, allowing the typical slug flow pattern of PHPs to occur. To provide a detailed insight on the thermo-hydraulics phenomena during the device start-up under the occurrence of microgravity, the PHP is equipped with a transparent sapphire tube insert, two miniature pressure transducers and two micro-thermocouples. The flow pattern and the liquid bulk temperature distribution are detected by a fast VIS camera and a medium wave IR camera respectively. The data recorded on the 67th ESA-NOVESPACE parabolic flight campaign are analyzed in the light of a future implementation on the ISS in 2020 and for the validation of actual numerical models. The device is continuously active during the whole microgravity periods without any stopover. The start-up tests (the heat power is provided after the 0-g occurrence) proved that the PHP operation is not primed by inertial effects. Finally, the thermal energy due to the sensible heat of the liquid phase is estimated showing a lower level than existing theoretical values.

Keywords: Pulsating Heat Pipe; International Space Station; Start-up; Microgravity; Parabolic Flight; Infrared Analysis.

1 INTRODUCTION

The thermal management of spacecrafts and satellites is a challenging issue, not only for the conditions of the open space (microgravity, vacuum, low temperatures), but also for the high standard levels in terms of compactness, weight, durability and heat transfer capability [1]. Various heat pipes (Grooved Heat Pipes, Sintered Heat Pipes, Loop Heat Pipes, Capillary Pumped Loops) have already been successfully used in aerospace applications [2]. In the last years, wickless two-phase passive devices, known as Pulsating Heat Pipes (PHP) or Oscillating Heat Pipes, are being studied in microgravity conditions too, due to their potential advantages in terms of flexibility, surface adaptability and low cost [3][9]. Gu et al. [3][4] were the first to speculate on the possibility to increase the PHP internal diameter so to increase the heat transfer capability. Indeed, in microgravity conditions, the ratio between buoyancy forces and surface tension forces decrease allowing to exploit larger diameter tubes with respect to the capillary limit on ground. This concept of large diameter PHP for space application was then tested both by means of parabolic flights [10][11] and sounding rocket [12] experiments proving that the device (inner diameter 3mm charged with FC-72) is responding to the occurrence of microgravity with a flow pattern transition from stratified to the slug-plug regime and that the flow pressure signal is exhibiting an oscillating trend throughout the entire 0-g period. On the other hand, due to the experimental assessments (mainly the system thermal inertia), it was not possible to reach steady state conditions. Therefore, it is essential to test the device in a long-term microgravity environment. In this framework, a large diameter PHP has been especially designed for the future implementation on the heat transfer host module (HTH) of the International Space Station (ISS). The condenser zone is cooled by means of a Peltier cell array, to reduce the response time linked to the thermal inertia, and the adiabatic zone is equipped with a sapphire tube for the simultaneous visualization and direct InfraRed (IR) analysis. Furthermore, local fluid temperature and pressure signals are acquired close to the evaporator and the condenser to investigate the PHP thermodynamic states during operation.

The present work describes the design process as well as the thermal characterization of this prototype under a varying gravity field during the 67th parabolic flight campaign by ESA/NOVESPACE. The main

objectives are:

a) Verify that the fluid motion is continuously active during the whole microgravity periods without any stopover.
b) Prove that the PHP operation is not primed by the flow inertial effect that may be already present before the microgravity period.
c) Show and quantify the fluid thermodynamic states of non-equilibrium in terms of vapor super-heating and liquid sub-cooling.
d) Show the feasibility of accurate temperature distribution measurements along liquid slugs by means of infrared analysis.

The outcome is vital for the refinement of the ESR (Experimental Scientific Requirements) document by our international PHP scientific team and for the validation of actual numerical models.

2 EXPERIMENTS

2.1 Test cell

The device is made of an annealed aluminum tube with an inner/outer diameter of 3/5 mm respectively. The closed loop is folded in a staggered 3D configuration with 14 turns in the evaporator zone as shown in **Error! Reference source not found.**. This geometry (220x80x25 mm) allows to fit the device in the very compact constraints of the HTH on the ISS. An aluminum T-junction on the top hosts one miniature pressure transducer (Keller® PAA-M5-HB, 1 bar abs, 0,2%FSO accuracy) as well as the vacuum and filling micro-metering valve (IDEX® Upchurch Sc. P-447).

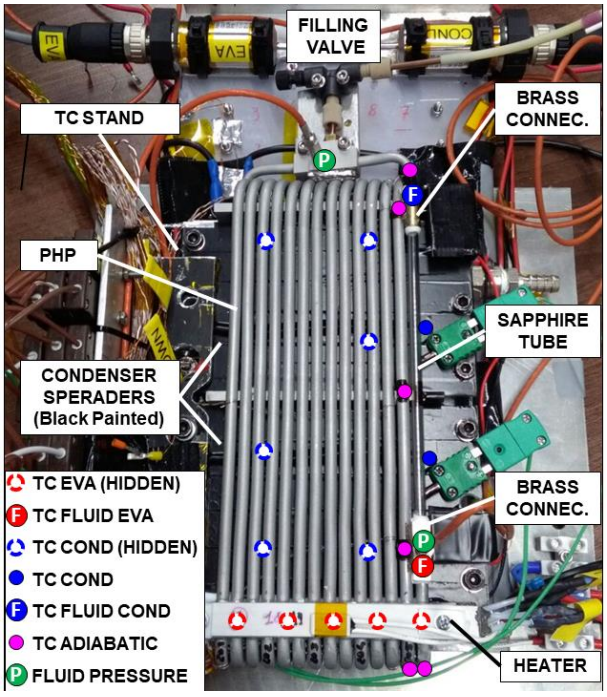

Figure 1: Test cell front view with thermocouples and pressure transducers location.

Two brass connections allow to connect a sapphire tube insert (Precision Sapphire Technologies®, length 140mm, same OD/ID of the aluminum tube) with the aluminum tube and to host two K-type micro-thermocouples (Omega® KMTSS-IM025E-150, bead diameter 0,25 mm, response time 0.1s with 95% confidence) for the fluid temperature measurement, as well as another miniature pressure transducer close to the evaporator section. Two aluminum spreaders (100x12x10mm) are brazed on the tube in the evaporator zone and host two ceramic ohmic heaters (Innovacera®, Electrical resistance 18Ω ±10%). The wall to fluid total heated area is 15.83 cm^2. The heating power is provided by a programmable power supply (GW-Instek®, PSH-6006A) from a minimum of 18W to a maximum of 180W, corresponding to an average wall to fluid heat flux from 1.10 to 11.43 W/cm^2. The condenser zone is embedded between two aluminum spreaders (80x120x10mm) cooled down by means of a Peltier cell system (8 Peltier cells by Adaptive Thermal Management®, ETH-127-14-11-S; control system by Meertstetter Engineering®, TEC 1123) coupled with a cold plate temperature control system loop (Aavid Thermalloy®). Five T-type thermocouples are located in between the evaporator spreader and the heater ($TC_{eva,hidden}$ in **Error! Reference source not found.**); eight are located between the Peltier cold side and the condenser aluminum spreader ($TC_{cond,hidden}$ in **Error! Reference source not found.**); two on the condenser spreader just behind the sapphire tube (TC_{cond} in **Error! Reference source not found.**); six are located on the tube external wall ($TC_{adiabatic}$ in **Error! Reference source not found.**). The device is partially filled with 22 ± 0.2 ml of FC-72 (50% vol.).

2.2 Peripheral facilities

The transparent section is investigated by means of a grey scale compact fast camera (Ximea® USB3 XIQ-093, resolution 1280x1024 pixel, up to 400 fps), and a high-speed and high resolution medium wave IR (AIM® from TEC-MMG, 1280x1024, 50fps, resolution 50mK, bandwidth 3-5µm, lens transmissivity 0.93). The high-speed camera is synchronized via software with the pressure signals and connected to an ultra-compact PC (Intel® NUC D54250WYB) storing images up to 200 fps. The IR camera is managed with his own PC and software borrowed by ESA. A data acquisition system (National Instruments®, NI-cRIO-9074, NI-9264, NI-9214, 2xNI-9205, NI-9217, NI-9472) is connected to a laptop and records the thermocouples and thermistors signal at 50Hz, and the pressure transducers signal at 200 Hz via a LabView® software. Table 1 shows the uncertainty related to all the measured parameters. All the thermocouples are calibrated by means of a thermal chamber

(BINDER®) and a reference four wire Pt-100 (ITS-90 standard, max. error 0.035 K).

Table 1: acquired parameters and uncertainties, TC relates to thermocouples, PT refers to the pressure transducers.

Parameter	type	Max error
Tube TCs	T	±0.1°C
Fluid TCs	K	±0.2°C
Fluid PTs	mini	±500 Pa
Fluid IR	Mid-Wave	±0.5°C
Power	134W	±3W

The IR temperature measurement is calibrated with a specific single-phase loop system using a Matlab algorithm described in [13]. The test cell, the 4 PC, the camera systems (greyscale and IR), the electrical and the cooling systems are mounted on a rack, made of aluminium beams and plates designed for being mounted aboard the Airbus A310, in compliance with the guidelines provided by Novespace [14].

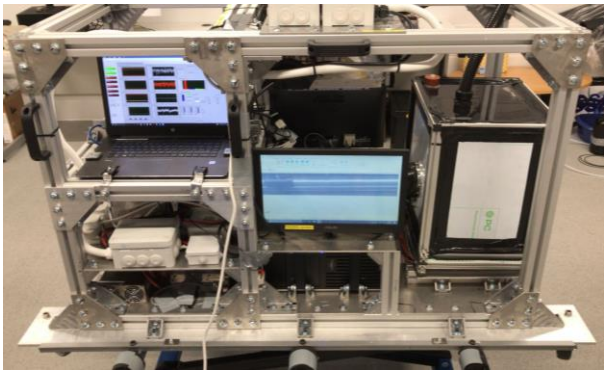

Figure 2: Experimental test rig for PF campaigns.

2.3 Experimental procedure

The 67th ESA-Novespace Parabolic flight campaign took place in Bordeaux in November 2017. During each of the three flight days, thirty-one parabolic trajectories are performed: the first one, called parabola zero, is followed by six sequences of five consecutive parabolae. In between each sequence, there are five minutes of steady flight at normal gravity level, used here to vary the heat power level and let the system reach a steady state when possible. Each parabola is composed by a first hyper-gravity period (20s at 1.8g), the microgravity period (20s at 0g) and a second hyper-gravity period equal to the first.

Table 2: Experimental matrix during the flight.

Parabola N°	DAY-I	DAY-II	DAY-III (start-up)
0	36W	18W	36W
1-5	52W	36W	36W
6-10	68W	52W	52W
11-15	96W	146W	-
16-20	134W	-	180W
21-25	68W	-	134W
26-30	52W	-	68W

The device has been tested in vertical position, bottom heated at eight different power levels (18, 36, 52, 68, 96, 134, 146, 180 W). As shown in Table 2, the first two days where devoted to the device thermal characterization, while the third to the investigation of the device start-up. During the thermal characterization, the device is heated up at the desired power level before the occurring of the microgravity period, and the power level is kept constant for the whole sequence, as already done in the previous parabolic flight campaigns [10][11]. During the third day the device is heated up after the occurrence of microgravity to prove that the PHP operation is not primed by the flow inertial effects, that may be still present before the microgravity phase. Each start-up test is repeated at least twice and, after each start-up, several parabolae are reserved to allow enough time for the whole system to cool down to the target temperature of the Peltier cold side, set to 20°C for all the experiments. Each microgravity period is recorded both with the greyscale and IR camera.

3 RESULTS

It is worthwhile to remind that the device is a hybrid system between a multiple evaporator loop ThermoSyphon (TS), when gravity acceleration is present, and a Pulsating Heat Pipe (PHP) in microgravity conditions as explained in [15]. The minimum power that primes a stable circulation during the TS mode in the present experiment is 68W, corresponding to a wall to fluid average heat flux of 4.29 W/cm^2, which is the same heat flux registered during the ground characterization of the 5 turns geometry [15]. To synchronize the gravity acceleration level with the heat input power level and the data of interest (temperatures, pressures etc.), the temporal trends are showed as the superposition of subplots. The delta pressure signal is the difference between the evaporator and the condenser pressure signal (black); the fluid temperature signals are shown on a separate subplot (red line for the evaporator, blue line for the condenser); the wall temperature signals of the evaporator and condenser spreaders are shown in reddish and blueish colors relatively, while the temperatures in the adiabatic zone are shown with purple colors. The microgravity period is highlighted with a semitransparent red band.

3.1 Thermal response to microgravity

As mentioned in the introduction, the microgravity period duration (about 20 s) is not enough to reach a pseudo steady state (i.e. when the mean value of the oscillating temperature signal is constant in time) , but it is very useful to investigate the device thermo-hydraulic response in different conditions and infer on the expected behavior in the long-term microgravity

environment available in the future experiments on the ISS. The response to microgravity condition is discussed separately for the first two days (constant heat input) and the third day (start-up).

3.1.1 Constant heat input

Similarly to previous microgravity experiments performed on a simpler geometry (5 heated zones) with the same fluid, internal diameter and heat flux levels [10][11], the activation of the flow motion or the change in the operational regime, is always detected by all the measurements, including the visualization, immediately after the occurrence of microgravity. The difference with respect to the pressure signal recorded for the simpler geometry is the absence of stopover periods which is a positive consequence of the larger number of heated zones.

At low heat fluxes (below 68 W), the vapor expansion is not able to prime the fluid circulation in the gravity assisted mode.

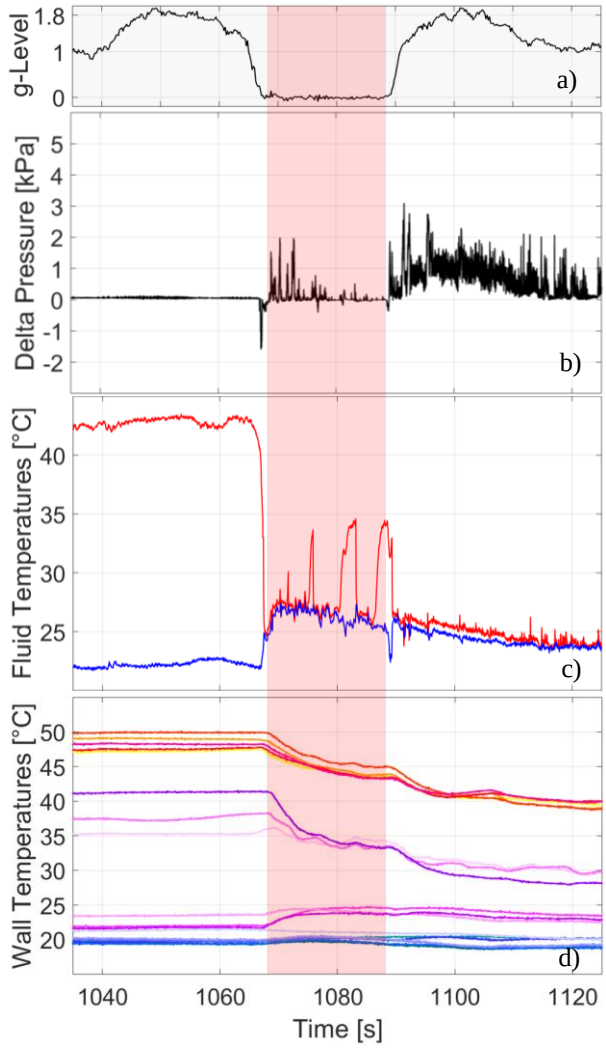

Figure 4: Delta pressure between the evaporator and condenser zone, fluid temperatures (red evap., blue cond.) and wall temperatures at constant power 36W.

Thus, the TS operation is characterized by frequent stopovers or even by the absence of flow motion. Figure 5b shows indeed that, during the first hyper-gravity level, when the heat power is 36W, the delta pressure between the evaporator and the condenser is zero and the fluid temperatures are steady (Figure 5c, d). With the occurrence of microgravity, the fluid ΔP shows several peaks (Figure 5b) and the fluid temperatures become instantaneously equal initially and then oscillate (Figure 5c, d). Consequently, the wall temperature at the evaporator decreases.

From 68W up to the maximum heat power input, when gravity is present, the fluid circulation is stable. This is clearly visible, not only from the greyscale visualization, but also from the fluid pressure and temperatures trends as shown in Figure 4. When the device is constantly heated at 180W, during 1g and hyper-g (TS mode), the delta pressure is always positive, while during microgravity (PHP mode) the fluid is oscillating without any stopover (Figure 4b), as also seen in a precursor experiment on the same geometry onboard a sounding rocket [12].

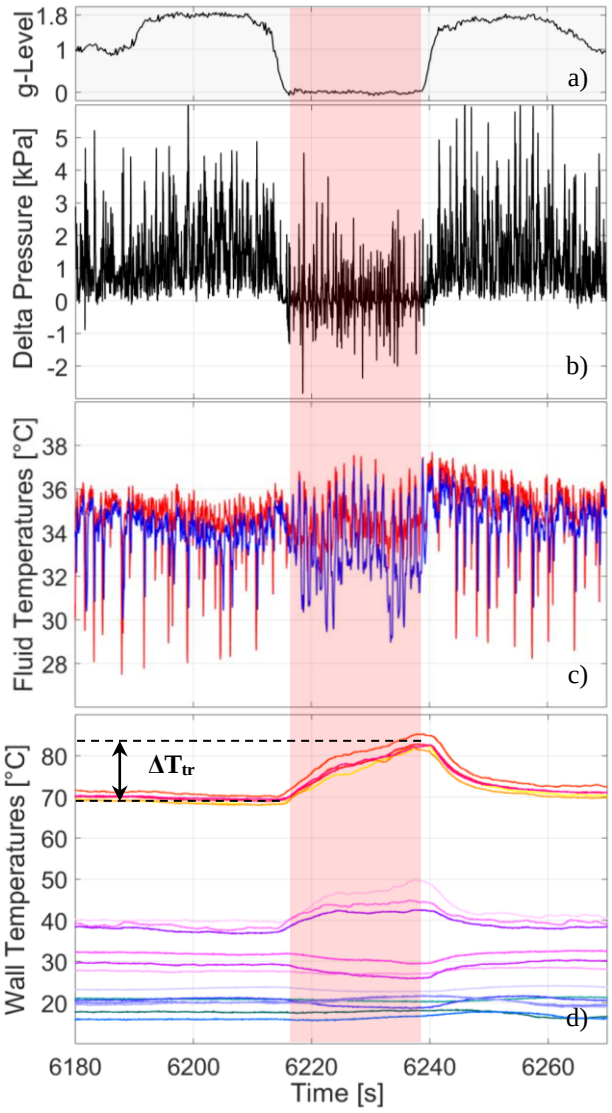

condenser, fluid temperatures (red evap., blue cond.) and wall temperatures at constant power 180W.

This last experiment on SR did not allow repeatability for obvious reasons.

The stable fluid circulation reached in TS mode during 1g and hyper-g allows the system to reach a pseudo steady state, as shown by the flat trend of all the temperature signals in **Error! Reference source not found.**d. The flow pattern transition from the annular circulating regime to the slug-plug oscillation, results in a decrease of the heat transfer rate and a consequent increase of the evaporator temperatures. The absence of stopover periods is anyway beneficial in comparison with the device with a smaller number of heated sections [10]. Indeed, for the same wall to fluid heat input flux, the temperature difference at the evaporator between the start and the end of the microgravity period in the present case is always smaller in comparison with the simpler geometry as shown in .

Table 3.

Table 3: Comparison between the evaporator temperature difference during the transient between the present work and previous experiments.

5 turns (Mangini et al. [10])		**14 turns (present work)**	
Q[W] - q" [W/cm²]	**ΔT_{trans} [K]**	**Q[W] - q" [W/cm²]**	**ΔT_{trans} [K]**
30 – 3.18	3	52 – 3.28	-
40 – 4.24	10	68 – 4.29	3
80 – 8.48	20	134 – 8.46	15
120 – 12.73	40	182 – 11.49	13

3.1.2 Start-up

The new tests performed with respect to previous experiments [10][11] consist in switching the power supply on immediately after the occurrence of microgravity. The main objective is to verify that the activation of the fluid motion is not primed by residual inertial effects due to the previous hyper-gravity period. The second objective is to understand the effect of the heat input level on the device start-up.

At low heat fluxes (36 and 52W) the duration of the microgravity period is not sufficient to reach the start-up. Only the fluid temperature signal at the evaporator shows some fluctuation, but all the other sensors, as well as the visualization, did not show any notable phenomenon. From 68 W, the fluid motion activation is clear from all the sensors as well as from the visualization and also repeatable. Figure 6 shows the device response at 182W. The subplot related to the power supply switch and the power input level is also added (Figure 6b). As per the lower heat flux levels, while the fluid is still not moving at all, the fluid temperature at the evaporator starts to show some activity (Figure 6d). Only when the fluid temperature at the condenser starts varying, the delta pressure starts oscillating (Figure 6c), and the slug/plug flow is also recorded by the cameras. The activation of the fluid, highlighted with a vertical dashed line, results in an increase of the overall heat transfer rate due to convection. Consequently, the temperature increase at the evaporator is also damped as shown in Figure 6e.

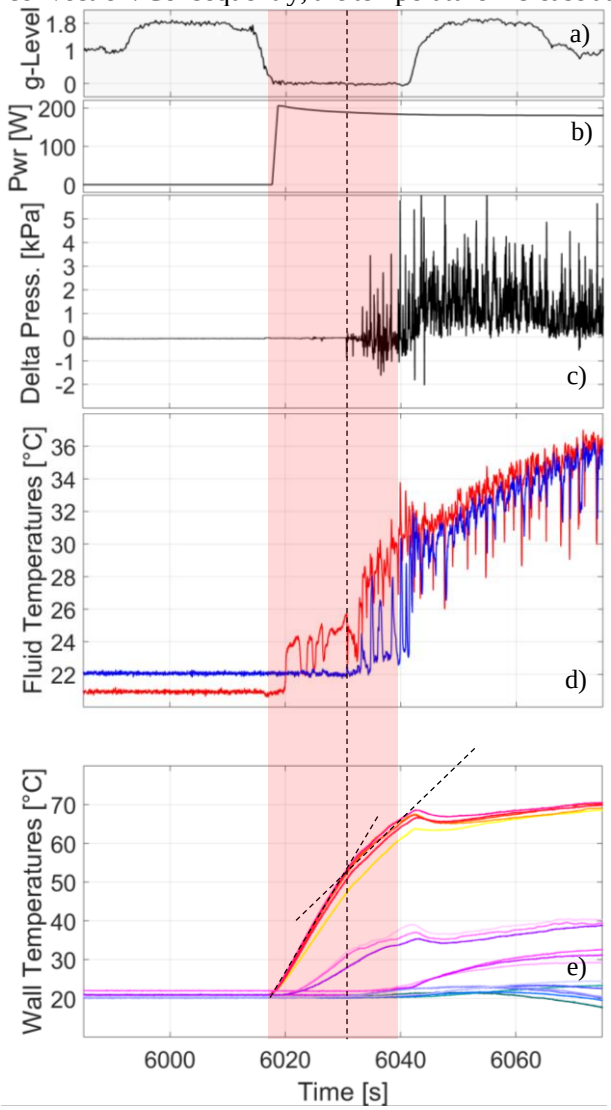

Figure 5: Delta pressure between the evaporator and condenser, fluid temperatures (red evap., blue cond.) and wall temperatures during start-up at 180W.

3.2 Non-equilibrium analysis

Many research papers in the literature assess that the local thermodynamic states of the fluid during the PHP operation may be far from the equilibrium conditions. There are experimental evidences on a single confined liquid–vapor inside a capillary channel [16][19] that the vapor within a bubble can be superheated, while less data is available concerning the subcooled state. The simultaneous fluid temperature and pressure measurements of the present experiment allows to compare the actual thermodynamic state with the saturated conditions and hence to infer on the super-heating and sub-cooling levels both close to the evaporator and to the condenser. At each time step, the fluid saturation temperature at the actual measured pressure $T_s(P_f)$ is

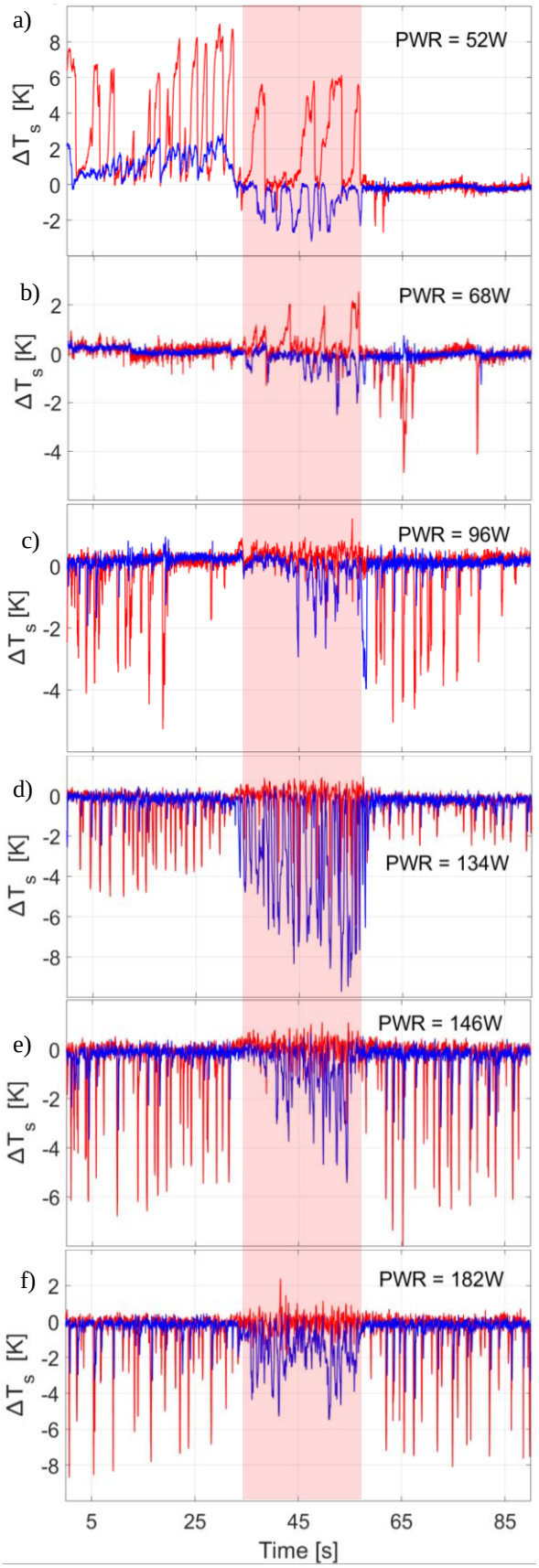

Figure 6: Saturation temperature differences during microgravity (semitransparent red band) at the different heat power levels (red: evaporator zone, blue: condenser zone).

calculated by means of the REFPROP 9.0 software released by NIST [20]. Then the difference between the measured fluid temperature T_f and the saturation temperature T_{sat} is calculated as follows:

$$\Delta T_s = T_f - T_{sat}(P_f) \quad (1)$$

When $\Delta T_s < 0$ the fluid is in subcooled conditions, for $\Delta T_s = 0$ the fluid is just saturated, when $\Delta T_s > 0$, the fluid is superheated. ΔT_s is shown at different heat input levels in Figure 7. At low heat inputs (Figure 7a), the flow motion is poor, the same fluid batches reside in the same location, resulting in large superheating levels at the evaporator and large sub-cooling at the condenser. Increasing the heat input, the flow oscillation is stronger and consequently the fluid batches reside in the same location for a shorter time. Consequently, the superheating at the evaporator decreases and it is always lower than 3K. Since the condenser surface is almost ten times the evaporator surface, the sub-cooling phenomenon is clearly recognizable at the condenser for all the heat input levels. But it is also present in the evaporator and increases both in amplitude and frequency with the heat input level.

Theoretically, the thermal energy transferred by the fluid in subcooled condition is due to the contribution of the sensible heat of the liquid phase, while the budget transferred when the fluid is saturated is due to phase change phenomena. Finally, the thermal energy transferred in superheated conditions is due to the sensible heat of the vapor phase. The three energy contributions to the overall thermal energy transfer with the heaters and the Peltier cells (the heat transfer at the adiabatic session is assumed negligible) can be defined as follows:

$$\begin{cases} E_{sub} = A\int_{t_0}^{t_{end}} h_{sub}(T_w - T_f)dt; & when\ \Delta T_s < 0 \quad (2) \\ E_{pc} = A\int_{t_0}^{t_{end}} h_{pc}(T_w - T_f)dt; & when\ \Delta T_s = 0 \quad (3) \\ E_{sup} = A\int_{t_0}^{t_{end}} h_{sup}(T_w - T_f)dt; & when\ \Delta T_s > 0 \quad (4) \end{cases}$$

And finally, the ratio between the sensible and the total thermal energy transfer:

$$\xi_{sub} = 100 \cdot E_{sub}/(E_{sub} + E_{pc} + E_{pc})\ \% \quad (5)$$

where T_w is the closest local temperature of the tube wall; h_{sub} and h_{pc} and h_{pc} are the instantaneous heat transfer coefficients in the subcooled, saturated and superheated conditions relatively; A is the wall-to-fluid heat transfer surface. The time domain (t_0, t_{end}) is the microgravity period.

Since the heat transfer coefficients, as well as the contribution related to sensible and latent heat, are unknown, it is not possible to provide an accurate absolute value of ξ_{sub}, but it is still possible to make a comparison with the theoretical values (not yet

experimentally validated) proposed by numerical models in the literature [21][22] which assess that the great majority (always more than 90%), of the heat transferred in a PHP is due to the sensible heat of the liquid phase. Assuming that for the same fluid, the same channel geometry and the same flow regime, the single-phase heat transfer coefficient is smaller than the one related to the phase change, in a "reductio ad absurdum" where the heat transfer coefficients are constant and equal:

$$h_{sub} = h_{pc} = h_{sup} = const \quad (6)$$

ξ_{sub} is no more dependent on the heat transfer coefficients and represents a physical maximum threshold. Indeed, if ξ_{sub} is bigger than the theoretical threshold value, h_{sub} should be bigger than h_{pc}, which is physically not consistent.

The percentage of the sub-cooling time with respect to the whole microgravity period is defined as:

$$\tau_{sub} = 100 \cdot t_{sub}/t_{tot} \ \% \quad (7)$$

ξ_{sub} and τ_{sub} are calculated for the present case both in the evaporator and the condenser during the microgravity period and shown in Table 4.

Table 4: Sensible over total thermal energy and sub-cooling over total time ratios for the evaporator and condenser during microgravity.

	68 W	**96 W**	**134 W**	**146 W**
$\xi_{sub,e}$ **[%]**	31.3	33.3	52.9	67.3
$\xi_{sub,c}$ **[%]**	31.5	22.2	48.8	66.9
$\tau_{sub,e}$ **[%]**	15.1	14.9	28.1	41.6
$\tau_{sub,c}$ **[%]**	59.1	54.5	79.6	89.8

The values are calculated only for the constant heat input levels where a stable circulation was achieved before microgravity and averaged on the different parabolae (the first of each sequence is excluded). Despite the thermal energy transferred via sensible heat is very consistent, the threshold values calculated here based on experimental data are always lower than the values proposed by [21][22]. This suggests that the two-phase phenomena are not only the main source of fluid momentum in terms of vapor production and bubble expansion, but they also remarkably contribute to the overall heat transfer. Since the values of ξ_{sub} are similar for the evaporator and condenser, but the ratio of sub-cooling time over the total is bigger for the condenser than the evaporator, the wall to fluid temperature differences in the evaporator are usually bigger than the condenser.

3.3 Infrared analysis

Infrared analysis can be a very powerful tool to investigate fast thermo-fluidic phenomena and thermal gradients along the liquid phase during the PHP operation. Given that the working fluid (FC-72) is semi-transparent to the mid-wave infrared radiation,

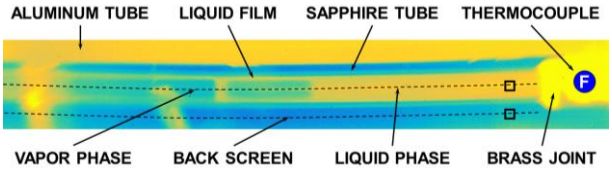

Figure 7: Infrared picture of slug flow during microgravity (black squares and dashed lines are the acquisition locations relatively for Figure 8 and Figure 9).

the fluid temperature can be accurately measured only when the liquid phase completely fills the channels (slug flow) and only when the backscreen and the ambient temperature are known [13].

Figure 8 shows an example of Infrared picture. The field of view is 80 mm, from the condenser brass joint on the right, to the middle of the tube on the left. The temperature scale goes from yellow (high) to blue (low). From left to right it is possible to recognize: the adjacent aluminum tube, the vapor phase, the liquid film, the back screen which is always colder than the fluid, the sapphire tube, the liquid phase, the brass joint and the thermocouple location. The calibration technique described in [13] consists in one separate single phase loop with the same tube geometry and fluid, where it is possible to control independently the fluid and the back-screen temperatures, equipped with accurate temperature sensors both for the fluid and backscreen. For each of the five different backscreen temperature levels (18, 20, 22, 24, 26 °C), the fluid temperature is varied from 5°C to 45°C with steps of 5°C. As soon as the system reaches the steady state, both the temperature signals coming from the thermal resistances and the IR images (20s at 50fps) are recorded. The data matrix is interpolated to obtain a transfer function able to provide the fluid temperature depending on the IR signal and the backscreen temperature.

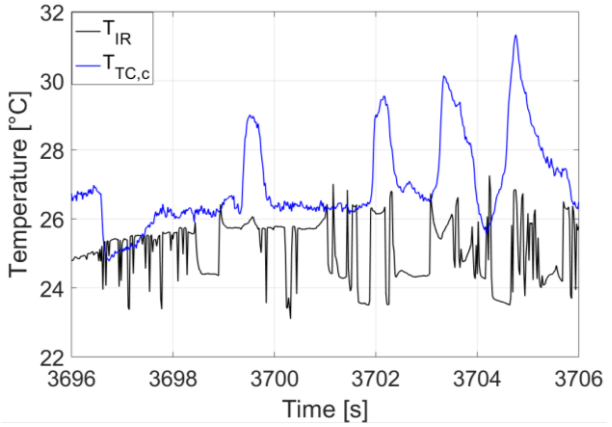

Figure 8: Fluid temperature temporal trend in a single location: comparison between infrared images (black) and thermocouple during microgravity start-up at 182W.

To check the level of accuracy of such technique, a 5x5 pixels window is selected both on the tube and the back screen as close as possible to the condenser

thermocouple location as shown in Figure 8. Then each image within a time sequence (20s at 50Hz) is processed with the calibration function matched with the condenser thermocouple. Figure 9 shows the comparison between the IR and the thermocouple signals during the last 10 seconds of microgravity after the start up at 182W. The two signals appear very different, but they can be interpreted in a physical way: the thermocouple signal is able to record both the liquid and vapor temperatures, so the temperature high peaks are due to the presence of superheated vapor. On the other hand, the IR measurement makes sense only if liquid is filling the channel completely. In case of vapor, since it is almost completely transparent to the IR spectrum, the camera is recording a temperature closer to the back-screen temperature as shown in Figure 8. This is the reason why only the lower values of the thermocouples and the higher values of the IR are relevant and comparable. The difference between the two signals in the relevant cases is always less than 0.5K, thereby

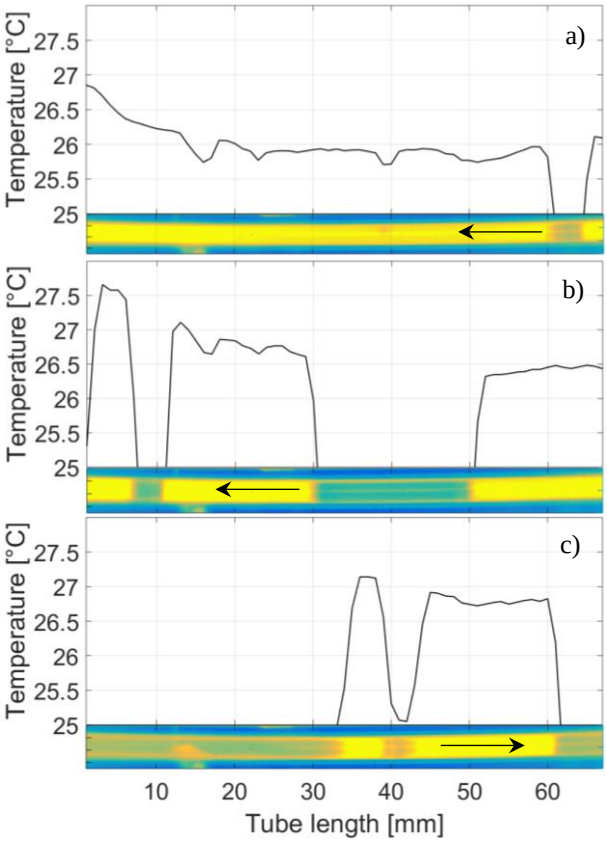

Figure 9: Fluid temperature along the tube axes in 3 subsequent time steps during 0-g start-up at 182W.

confirming that the IR accuracy on the liquid temperature for the present case is ± 0.5K.

The above analysis is extended to the entire field of view to provide the temporal trend of the liquid slug temperature distribution. The pixels in the tube mid axis and along the back-screen below the tube (dashed lines in Figure 8) are processed via the calibration tool and the temperature distribution is plotted together with the related thermogram to creating a video sequence. Here, only three subsequent time steps are shown in Figure 10. The flow direction is indicated with a black arrow on the IR image. The temperature resolution of the camera (50 mK) allows to detect the temperature gradient along the liquid slugs. Since the left side is closer to the evaporator and the right is closer to the condenser, the temperature decreases along the slug from left to right (Figure 10a). The effect of the wall thermal distribution on the fluid is also recognizable by matching two subsequent time stamps: the liquid slugs warm up is indeed evident from Figure 10a to b while the liquid slug is cooling down from Figure 10b to c.

4 CONCLUSIONS

The thermal characterization of a hybrid TS/PHP prototype under a varying gravity field is presented here to prove the feasibility of a future experiment onboard the International Space Station. The device is equipped with temperature and pressure sensors as well as with a transparent sapphire insert for the simultaneous visualization and non-intrusive temperature distribution measurements. The main research outcomes are listed here below:

- The fluid motion is continuously active during the whole microgravity periods without any stopover.
- In comparison with a previous experiment with a smaller number of heated sections [10], the absence of stopover periods is beneficial in terms of heat transfer rate. Indeed, for the same wall-to-fluid heat input flux, the temperature difference at the evaporator between the beginning and the end of the microgravity periods is always smaller in the present case.
- The start-up tests (the heat power is provided after the occurrence of microgravity) prove that the PHP operation is not primed by the flow inertial effect still present if the device is also operational before the microgravity period.
- The existence of non-equilibrium thermodynamic states is quantified in terms of vapor super-heating and liquid sub-cooling, both at the evaporator and the condenser zones. Using an “ad absurdum” assumption, the maximum level of thermal energy due to the sensible heat of the liquid phase is logically predicted as being much lower than existing theoretical estimations.
- Accurate temperature distribution measurements along liquid slugs by means of infrared analysis are possible and provide valuable data for the validation of theoretical and numerical models.

ACKNOWLEDGEMENTS

The present work is carried forward in the framework of the ESA MAP Project INWIP and the EPSRC UK HyHP Project (EP/P013112/1). Thanks to the NOVESPACE team in Bordeaux, and especially to Ms. A. Jacquemet for their ground and flight technical support. Thanks to Roberto Manetti, Massimo Ciampalini, Franco Peticca, Davide Della Vista for their essential technical contribution and to Marco Bernagozzi and Matteo Pozzoni for their support and the participation to the campaign. Special thanks to Dr. B. Toth for his constant interest and support. Furthermore, the team would like to thank the TRP project, and the laboratory TEC-MMG at ESA/ESTEC for lending the MWIR camera.

NOMENCLATURE

A : Area (m^2)
E : Energy (J)
h : Heat transfer coefficient (W/ m^2K)
ξ : sensible (liq.) over total thermal energy (%)
P : Pressure (kPa)
t : Time (s)
T : Absolute temperature (K)
τ : sensible (liq.) over total time (%)

Subscripts

c : Condenser
e : Evaporator
end : End of the microgravity period
f : Fluid
IR : InfraRed
pc : phase change (evaporation/condensation)
s : Saturated conditions
sub : Subcooled conditions
sup : Superheated conditions
TC : Thermocouple
tot : Total
tr : Transient
w : Wall
0 : Start of the microgravity period

REFERENCES

[1] Gilmore, D. G., Spacecraft Control Handbook, Fundamental Technologies, Second Edition, Vol. 1, The Aerospace Corp., AIAA Publ., (2002).

[2] Sunden, B., Fu, J., Heat Transfer in Aerospace Applications, Academic Press, (2017) 117-144.

[3] Gu, J., Kawaji, M., Futamata, R., Effects of gravity on the performance of pulsating heat pipes, *J. Thermophys. Heat Trans.* 18 (2004) 370–378.

[4] Gu, J., Kawaji, M., Futamata, R., Microgravity performance of micro pulsating heating pipe, *Micrograv. Sci. Technol.* 16 (2005) 179–183.

[5] De Paiva, K.V., Mantelli, M.B.H., Slongo, L.K., Burg, S.J., Experimental tests of mini heat pipe, pulsating heat pipe and heat spreader under microgravity conditions aboard suborbital rockets, *Proc. of the 15th IHPC, Clemson, South Carolina, USA*, 2010.

[6] De Paiva, K.V., Mantelli, M.B.H., Florez, J.P.M., Nuernberg, G.G.V., Mini heat pipe experiments under microgravity conditions. What have we learned? *Proc. of the 17th IHPC, Kanpur, India*, 2013.

[7] Mameli, M., Araneo, L., Filippeschi, S., Marelli, M., Testa, R., Marengo, M., Thermal performance of a closed loop pulsating heat pipe under a variable gravity force, *Int. J. Ther. Sci.* 80 (2014) 11–22.

[8] Ayel, V., Araneo, L., Scalambra, A., Mameli, M., Romestant, C., Piteau, A., Marengo, M., Filippeschi, S. Bertin, Y., Experimental study of a closed loop flat plate pulsating heat pipe under a varying gravity force, *Int. J. Therm. Sci.* 96 (2015) 23–34.

[9] Taft, B.S., Laun, F.F., Smith, S., Microgravity performance of a structurally embedded oscillating heat pipe, *J. Thermophys. Heat Transfer* 29 (2) (2015).

[10] Mangini, D., Mameli, M., Geourgoulas, A., Araneo, L., Filippeschi, S., Marengo, M., A pulsating heat pipe for space applications: ground and microgravity experiments, *Int. J. Therm. Sci.* 95 (2015) 53–63.

[11] Mangini D., Mameli M., Fioriti D., Araneo L., Filippeschi S., Marengo M., Hybrid Pulsating Heat Pipe for Space Applications with Non-Uniform Heating Patterns: Ground and Microgravity Experiments, *App. Therm. Eng.* 126 (2017) 1029–1043.

[12] Nannipieri P., Anichini M., Barsocchi L, Becatti G., Buoni L., Celi F., Catarsi A., Di Giorgio P., Fattibene P. Ferrato E., Guardati P., Mancini E., Meoni G., Nesti F., Piacquadio S., Pratelli E., Quadrelli L., Viglione A. S., Zanaboni F., Mameli M., Baronti F., Fanucci L., Marcuccio S., Bartoli C., Di Marco P., Bianco N., Marengo M., Filippeschi S., Upgraded Pulsating Heat Pipe Only For Space (U-Phos): Results Of The 22nd Rexus Sounding Rocket Campaign, *9th ExHFT*, 12-15 June, 2017, Iguazu Falls, Brazil.

[13] Catarsi A., Fioriti D., Mameli M., Filippeschi S., Di Marco P., Accuracy Analysis of Direct Infrared Temperature Measurements of Two-Phase Confined Flows, 16th International Heat Transfer Conference, IHTC-16, August 10-15, 2018, Beijing, China.

[14] Gai F., Experiment Design Guidelines in Parabolic Flight, GDL-2016-01, NOVESPACE 15, rue des Halles 75001 Paris – France.

[15] Mameli M., Mangini D., Vanoli G., Filippeschi S., Araneo L., Marengo M., Advanced Multi-Evaporator Loop Thermo-syphon, *Energy*, 112 (2015) 562–573.

[16] Bonnet F., Gully P., Nikolayev V., Experimental study of a single branch cryogenic pulsating heat pipe: first results, Proc. Eurotherm Sem. On Gravitational Effects on Liquid–Vapour Phase Change, IUSTI, Hyeres, France, 2011.

[17] Gully P., Bonnet F., Nikolayev V., Luchier N., Tran T.Q., Evaluation of the vapour thermodynamic state in PHP, Proc. 17th International Heat Pipe Conference, IIT Kanpur, Kanpur, India, 2013.

[18] Rao M, Lefevre F, Khandekar S, Bonjour J., Understanding transport mechanism of a self-sustained thermally driven oscillating two-phase system in a capillary tube. Int J Heat Mass Transf., 2013; 65:451e9.

[19] Rao M, Leevre F, Khandekar S, Bonjour, Mechanisms of a self-sustained thermally driven oscillating Liquid-Vapour meniscus. Int J. Heat Mass Transf 2015; 86:519e30.

[20] Lemmon E.W., Huber M. L., McLinden M. O., NIST Standard Reference Database 23: Reference Fluid Thermodynamic and Transport Properties-refprop, Version 9.0, National Institute of Standards and Technology, Standard Reference Data Program, Gaithersburg Maryland 20899, 2013.

[21] Shafii M.B., Faghri A., Zhang Y., Thermal modeling of unlooped and looped pulsating heat pipes, J. Heat Transfer 123 (2001) 1159–1172.

[22] Shafii M.B., Faghri A., Zhang Y., Analysis of heat transfer in

unlooped and looped pulsating heat pipes, Int. J. Numer. Meth.
Heat Fluid Flow 12 (5) (2002), 585–609.